Nanofluidic platform for templating, reacting, and visualizing single biopolymers in real time

Gil Henkin, Daniel Berard, Frank Stabile, Jason S. Leith, and Sabrina R. Leslie

Received Xth XXXXXXXXXX 20XX, Accepted Xth XXXXXXXXX 20XX
First published on the web Xth XXXXXXXXXX 200X
DOI: 10.1039/b000000x

We present a controlled nanofluidic device for visualizing, manipulating, and reacting confined biopolymers under a broad range of physical and imaging parameters. This device enables temporally controlled reagent insertion within nanoscale spaces, an outstanding challenge to existing biotechnology and biophysical tools. It functions by first confining and formatting polymer conformations within embedded nanostructures from the top, using the principle of Convex Lens-induced Confinement (CLiC), and second immersing these polymers in reagents, with minimal disturbance, using a deep embedded microgroove. To demonstrate this platform, we confine and extend DNA polymers within a central nanogroove array, and temporally resolve changes in extension and brightness in response to dynamically exchanging the buffer. Second, we visualize and characterize condensation of nanogroove-extended DNA polymers in response to introducing surfactant molecules in solution. Third, under applied heat and denaturation conditions, we resolve single Cy3B-conjugated oligonucleotide probes bind to locally melted, single-stranded regions of lambda-phage DNA. This platform's all-glass confining environment is quantitatively known, adjustable to the nanometer level, repeatable, and non-porous to contamination; these are features to actualizing new biophysical studies and biotechnologies with high throughput and extended imaging conditions.

1 Introduction

As microscopy has advanced to the point of single-molecule resolution, there is great interest in visualizing and studying biological mechanisms at the nanoscale. The dynamic change in structural properties of DNA molecules in response to modified biochemical environments, especially subject to crowding and confinement, present a subject of particular interest within biological as well as biotechnological research contexts [1–3]. Single-molecule microscopy of DNA molecules undergoing dynamic processes inside nanoscale volumes, such as compaction or interactions with proteins, can provide mechanistic insights into physiological processes within the nucleus. Furthermore, single-DNA manipulation and visualization techniques are at the forefront of next-generation DNA sequencing methodologies, which seek to gently handle, treat, and analyze delicate, genomic material in miniature devices [4–7]. Existing approaches to probing dynamic biomolecular processes with single-molecule resolution face challenges in simultaneously achieving high throughput, temporal control over introducing reagents inside nanofluidic environments and visualizing the system response – particularly because this involves overcoming several orders of magnitude of applied confinement, precise control over the confining geometry, and access to a wide range of imaging timescales and reagent concentrations [2,7]. Performing single-molecule measurements is critical to detecting rare events and identifying subpopulations, which might otherwise be lost in ensemble averages. High throughput is essential to reaching quantitative conclusions in the presence of levels of stochastic noise associated with physiological systems. Establishing precise control over the environment experienced by biomolecules during analysis enables their interactions and concentrations to be well known and reproducible [8].

Prior single-molecule microscopy studies of molecular interactions have often used surface-immobilized DNA molecules for convenience of data collection and analysis. However, surface-attachments can restrict the accessible range of molecular configurations, especially during dynamic processes of interest, as well as introduce complications in sample preparation and data interpretation. While Total Internal Reflection Fluorescence (TIRF) microscopy has enabled exquisite visualization of interactions between surface-immobilized molecules and freely diffusing molecules, providing many important biophysical insights [9,10], these measurements can be limited by surface and tethering effects, by low accessible concentrations of diffusing species (due to added background), and by short per-molecule trajectories of diffusing species (due to escape from the detection volume). Optical [11,12] and magnetic [12,13] tweezers and Atomic Force Microscopy (AFM) [12,14] have provided complementary force and fluorescence measurements during reactions, but are typically limited in throughput and in accessible imaging conditions.

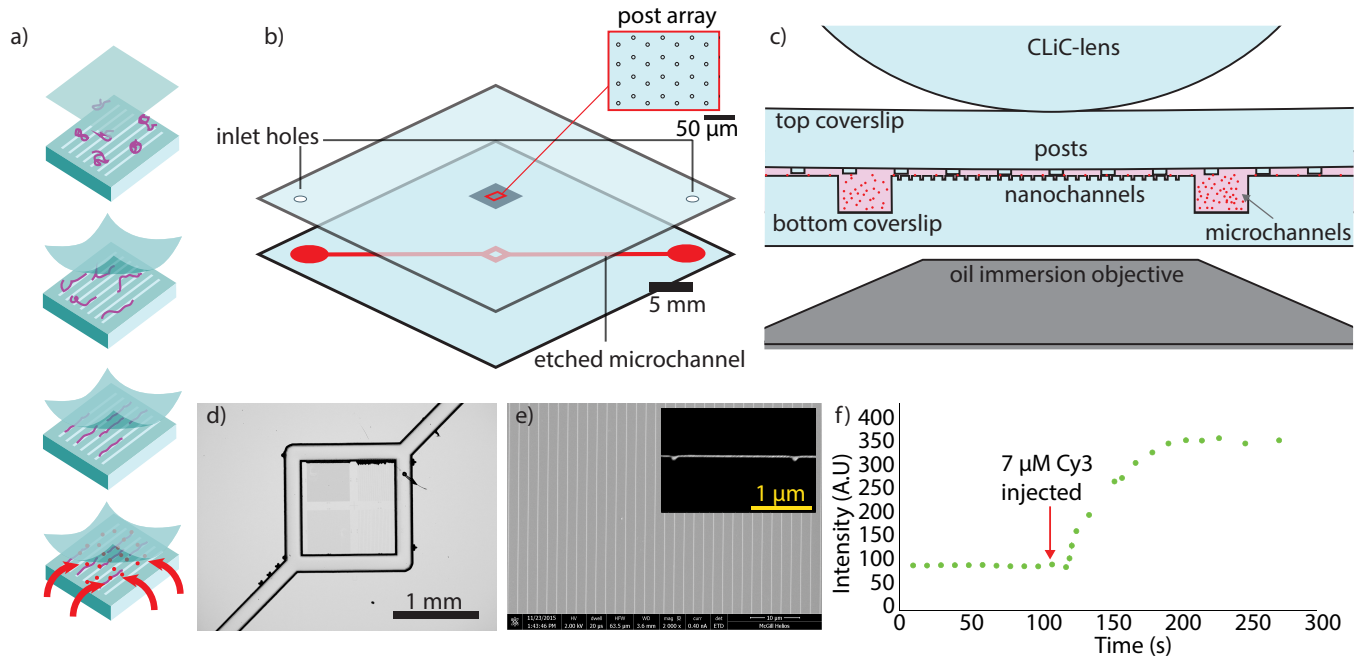

Fig. 1 Device images and schematics (not to scale). **a)** Schematic of CLiC confinement of DNA molecules. The top surface is deformed downwards and forces the sample molecules into a thin slit. When the slit height approaches the 50-nm persistence length of DNA polymers, DNA are observed to enter the embedded 50-nm cross-section grooves. **b)** Schematic of micro- and nanofluidic flow cell. The bottom surface contains a deep microchannel (30-micron cross section) which encircles a central array of nanochannels (50-nm cross section). The top coverslip contains a central millimeter-scale array of posts with 10-micron diameter, 30-micron spacing, and 20-nm height. Inlet holes sandblasted into the corners of the top glass coverslip enable sample insertion and removal. The two coverslips are held together by double-sided adhesive with 10-micron thickness. **c)** Side-view of device. **d)** Optical microscope image of the central nanochannel array and encircling microchannel. **e)** SEM image of nanochannel array, with nanochannel profile inset. **f)** Fluorescent intensity of the central CLiC region (82 × 82 microns) after introduction of Cy3 fluorescent dye, excited with a 532-nm laser.

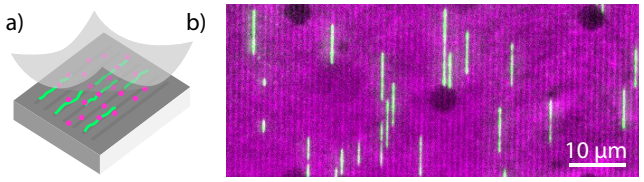

Fig. 2 a) Schematic of DNA polymers (green) confined to nanochannels in a buffer containing a fluorescent dye (magenta). **b)** False-color fluorescent image of confined YOYO-1–stained λ-phage DNA (green) in buffer containing Cy5 dye (magenta), illuminated with 488- and 657-nm wavelength excitation lasers; this super imposes spectrally-separate fluorescence images captured using a dual-view system. The fluorescent dye is excluded by the posts, corresponding to dark circles in the image.

A range of micro- and nanofluidic and fabrication approaches have been developed to achieve sub–persistence-length confinement of DNA and other polymers. By extending DNA polymers in nanochannels, genomic features may be mapped to position along the DNA length[15], of great interest sequencing and mapping industries. Visualizing interactions between extended DNA and biomolecules allows sequence-specific processes to probed and understood, such as targeted labeling[16,17] or binding[18] or cleavage[19]. However, since existing nanofluidic approaches typically apply high pressure or electrophoresis to drive polymers into enclosed nanochannels from the side, they risk breaking long DNA into fragments, risk clogging and are sensitivity to device surface roughness, and make temporally controlled introduction of reagents challenging[20–22]. TIRF visualization platforms typically use applied flow to extend DNA during experiments, meaning that reagents are also under constant flow. Relative to glass, PDMS-based microfluidics face challenges in reaching nanoscale dimensions, are vulnerable to contamination by reagents due to being porous, and have higher autofluorescence[23].

In this work, we introduce a new platform for high-throughput visualization of reactions betweened confined biopolymers and biomolecules, under adjustable nanoscale

confinement (provided by smooth glass walls with embedded nanotopographies) and with temporally controlled reagent insertion, opening the door to a broad range of applications. It uses and extends Convex Lens-induced Confinement (CLiC) technology to enable single-molecule visualization under an extended range of concentrations and observation times (Fig. 1)[24,25].

The CLiC technique addresses the challenge of overcoming several orders of confinement in loading delicate DNA polymers and complexes into small spaces by gently loading the polymers into open-face grooves from the top. In this work, we introduce a deep microchannel encircling the nanofluidic imaging region to insert reagents into this region from the side by diffusion, without disturbing the templated polymers.

As shown in Figure 1, our device uses a flow-cell formed of two coverslip surfaces which contain embedded topographies on both nanometer and micron lengthscales. The top flow-cell surface contains a dilute array of nano-scale post extrusions (typically 20nm tall) which provide a slit through which reagents can be exchanged. During CLiC imaging, a convex lens, curve-side down, presses the top chamber surface downward and can come into contact with the bottom surface. Of special importance during reagent exchange, the contact achieved between the posts and bottom coverslip provide mechanical stability and spatial homogeneity to the imaging chamber height over a large area; this corresponds to a few 50-100 μm square fields of view in this study, but is extendable by e.g. increasing size of the post-array and further deforming the chamber roof. The bottom surface contains embedded linear nanogrooves (typically 40 to 50 nm deep) into which DNA polymers can be templated in an extended form as the CLiC-lens is lowered. The overall vertical confinement felt by a polymer within the nanochannel is less than 70 nm, a regimne in which potential loops in the extended DNA conformations are highly suppressed [26].

By fabricating nanogrooves of different topologies, polymer configurations can be controlled prior to inserting reagents. A deep microchannel (typically 30-micron cross-section) is embedded in the chamber floor, encircling the nanogroove array and imaging region. Since hydraulic resistance in response to pressure scales as the cube of the applied confinement[27], inserting reagents and applying flow within the microchannel results in negligible disturbance to DNA pre-loaded in the nanoslit and nanogrooves. This device decouples the initial confinement of DNA polymers from their subsequent interaction with reagents and biomolecules and allows subsequent morphological effects of the interactions to be visualized inside the nanogrooves.

Among these interactions is the compaction of DNA by a surfactant. DNA compaction is a fascinating problem with biological consequences. The human genome, for example, is about 2 meters in end-to-end length, and must compact itself into each cell nucleus about 10 microns in diameter, a reduction in scale by several orders of magnitude[28]. There is much interest in how this transition comes about, and many methods to recreate such an effect *in vitro* with controlled, few-component systems. Interestingly, despite the variety of approaches to achieving DNA condensation—surfactants, divalent salts, molecular crowding—the condensed conformation is revealed to be almost universal, a tightly coiled toroid[29]. In this work we demonstrate a the use of CLiC to resolve the temporal and spatial properties of compaction dynamics that would be hidden in bulk or in AFM/SEM studies.

2 Materials and Methods

2.1 Device design and fabrication

Our reaction-visualization device is composed of two coverslips with etched micro- and nano-scale features, which are held together by laser-cut double-sided adhesive. Embedded features are etched using standard wafer-scale microfabrication techniques; in particular, electron-beam lithography, contact UV lithography, and wet and dry etches are used. The top coverslip is patterned with a 2mm-square hexagonal array of short (20–50 nanometer) circular posts, 10 microns in diameter and spaced by 30 microns, etched via contact lithography and reactive ion etch (RIE). In the assembled flow cell, this array sits above above open-face nano-scale features in the bottom coverslip. Nanochannel arrays as large as 1mm-square are positioned in the center of the coverslip, etched with electron beam lithography and RIE. Spacing between nanochannels varies between 2 and 8 microns, each array about 500 microns square. The nanochannels are typically 50-nm in cross section, intended to reach Odijk confinement of DNA polymers[32].

Surrounding this central 1.2-millimeter-square region is a microchannel 200 microns wide, 30 microns deep, etched with contact lithography and treated with an HF wet etch. As shown in Fig. 1, it is extended to run between two corners of the coverslip, which are positioned below 3-millimeter holes in the top coverslip to enable sample insertion and removal. The flow-cell is sealed to a fluidic chuck using thumbscrews and a silicone rubber gasket fixing it to the CLiC instrument, which is mounted atop an inverted fluorescence microscope. Prior to imaging, the CLiC-lens is centered on the post array. As the roof is deformed downward and into contact, the post array offers a consistent stand off between the coverslips. Critically, it suppresses the confinement gradient across the trapped biopolymers and provides stable confinement during solution exchange.

2.1.1 Posts and top coverslip. First, the top coverslip inlet holes are sandblasted. Piranha-cleaned (see 2.2.1, "Cleaning procedures") sandblasted coverslips are then patterned with

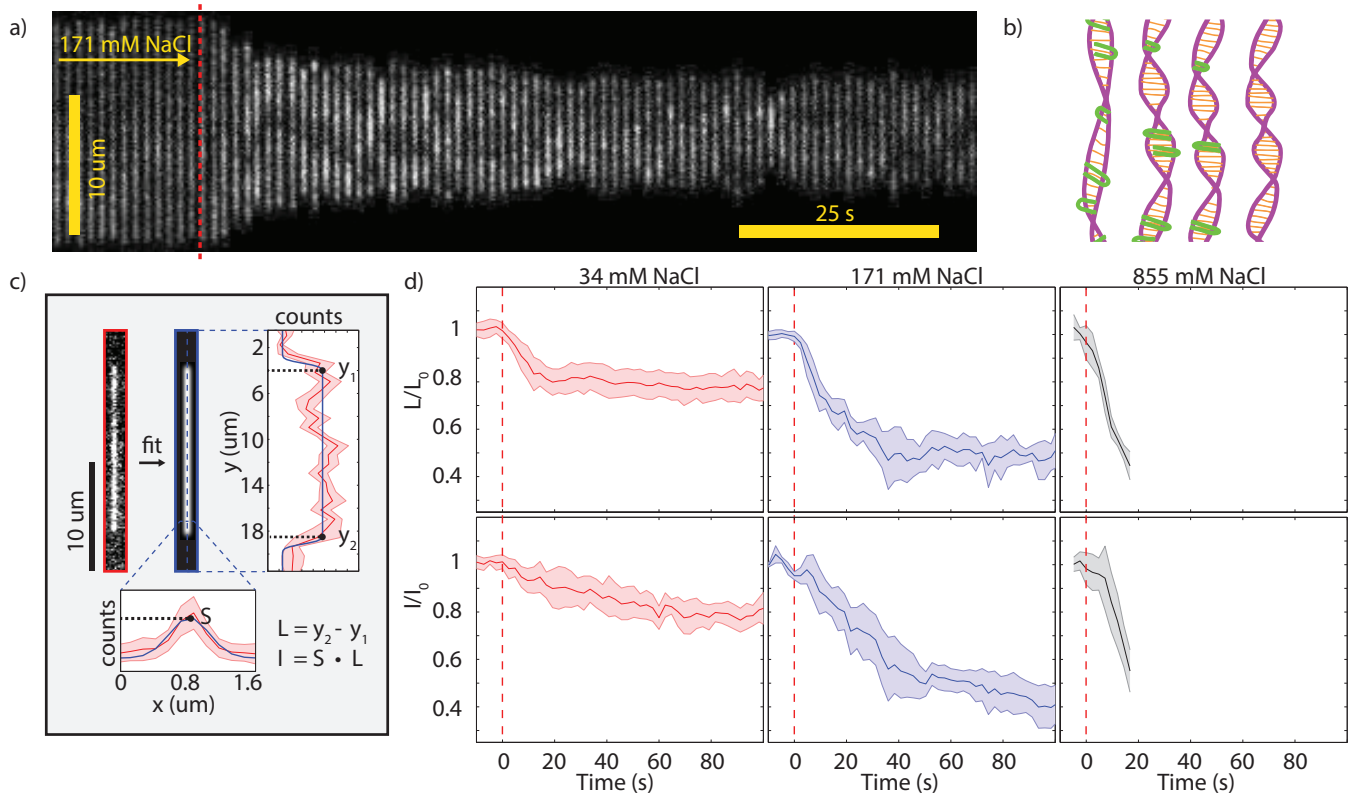

Fig. 3 DNA extension and intensity in response to buffer exchange of variable ionic strength. **a)** Kymograph of a confined YOYO-1–stained λ DNA molecule in response to buffer exchange which results in an increase in ionic strength from 0 to 171 mM NaCl. The red dashed line indicates the time at which the buffer was exchanged. **b)** Schematic of proposed mechanism of DNA extension and intensity changes under increased ionic strength. The negative charges along the length the DNA molecule (purple) are screened, decreasing persistence length. At the same time, the intercalated YOYO-1 molecules (green), which are electrostatically coupled to the backbone, dissociate [30,31]. **c)** Example of fitting procedure for extracting DNA length and fluorescent intensity from experimental data. **d)** Plots of normalized length and intensity of 6 to 10 DNA molecules for three experiments, each increasing from 0 to 34, 171, or 855 mM NaCl. The red dashed line shows when the buffer is exchanged. Introducing the highest salt buffer (855 mM NaCl) caused the DNA intensity to drop below background within 20 seconds and eventually deposit on the surface. At lower salt concentrations the DNA molecules were diffusing within the grooves.

a dilute hexagonal array of 10 micron wide circles in SU-8 negative resist. The glass is subsequently placed in an RIE chamber for CF_4/CHF_3 etching of 20 nm of glass, leaving the hexagonal array as extrusions on the surface.

2.1.2 Nanochannels and bottom coverslip. Piranha-cleaned D263 glass wafers are patterned with gold alignment marks by standard UV lithography and sputtering. After a plasma clean, the coverslips are spincoated with ZEP, a positive resist sensitive to exposure to electron beams, and coated with evaporated aluminum for a discharge layer. The ZEP is exposed using electron-beam lithography to define nanochannel arrays, with 500-micron by 50-nanometer nanochannels spaced by 1–8 microns. The exposed pattern is then developed and etched for depths of about 50 nanometers.

2.1.3 Microchannels. Microchannels are etched on clean coverslips that were previously patterned with nanochannel arrays. Sequentially sputtered chromium and gold is etched using UV lithography of S1813 photoresist followed by metal etchants to create an etch mask. HF subsequently etches the exposed glass to a depth of 30 microns.

2.2 Surface preparations

2.2.1 Cleaning procedures. Each coverslip undergoes a rigorous cleaning procedure before use. Because the flow cells are recovered and reused between experiments, residues must be removed. We treat coverslips in sequential baths of KOH in ethanol at room temperature, Hellmanex at 50° C, acetone at 50° C, and finally isopropanol at 50° C to remove macroscopic residues, followed by a clean in 3:1 sulfuric acid

to 30% hydrogren peroxide piranha solution to thoroughly remove any organics from the surface and expose hydroxyl groups. Coverslips are rinsed thoroughly with DI water between all steps. Coverslips are then soaked in 100mM KOH, rinsed with DI water, and are ready for use or for further treatements. Since CLiC microscopy requires good surface contact, rigorous cleaning is essential.

2.2.2 Silanization. For experiments requiring a particularly inert surface, coverslips are next treated with 1H,1H,2H,2H-Perfluorooctyldimethylchlorosilane (FOCS) prior to use. Coverslips are placed in a vacuum dessicator for one hour with 5–10 μL of FOCS for vapor-phase deposition. The coating can be assessed by examining the shape of a water droplet on the coverslip; a successful coating yields a highly hydrophobic surface.

2.3 DNA samples.

For most experiments, λ-phage DNA is initially diluted from 500 ng/μL stock solution to 200–500 ng/μL, and added to an equal volume of 33.2 μM YOYO-1 dye to achieve a mixture in solution of 1 dye molecule for every 10 basepairs. All solutions are diluted in 0.5x TBE. The mixture is incubated for an hour for uniform dye distribution. The stained DNA is stored at this concentration of 100 ng/μL and subsequently diluted for experiments. For experiments with cationic surfactants that compete with YOYO-1 for negative charges along the backbone, we instead stain with a Mirus Cy3 LabelIt kit, which covalently attaches cyanine-3 molecules to guanines along the length of the DNA.

2.4 Microscopy experiment.

Immediately prior to a microscopy experiment, fluorescently labeled DNA is diluted from 100 to 50 ng/μL in 0.5x TBE that is previously mixed with 6% β-mercaptoethanol (BME, for YOYO-1–labeled DNA) by volume, or 768 μg/mL protocatechuic acid (PCA) and 68 μg/mL protocatechuate-3,4-dioxygenase (PCD), for Cy3-labeled DNA.

A flow-cell assembled with 10-μm double-sided adhesive is placed on a sample plate above the inverted fluorescence microscope, and sealed to a microfluidic chuck with a rubber gasket and thumbscrews[25]. The chuck allows sample loading by applied air pressure at the inlet and outlet holes. The tube holding the CLiC-lens is mounted above the chuck and is lowered by a stepper motor (for coarse control) and piezo (for fine control), after the flowcell is positioned underneath the lens by a custom translation stage controlled by micrometers.

For experiments using Cy3-labeled λ DNA, the chamber was washed with 30 μL of 10% 5-kDa polyvinylpyrrolidone (PVP) with the PCA/PCD oxygen scavenging system, and then incubated for 15 minutes before rinsing with 60 μL of 1% 55-kDa PVP[25].

The diluted fluorescently labeled DNA is loaded into the chamber and the CLiC lens is lowered by the piezo until contact is made between the posts and the bottom coverslip, indicated by imaging the interference pattern of the laser excitation: when glass is in contact, the central region will become dark and remain dark with further lowering of the CLiC lens. After contact is made, the CLiC lens can be lowered an additional 10 to 15 μm to further deform the glass and ensure contact across an extended area[25]. Using a 488-nm laser for YOYO-1 excitation or 532-nm laser for Cy3 excitation, and standard emission filters for these fluorophores' spectra, the DNA extension in nanogrooves can then be observed using an EM-CCD camera (Andor iXon Ultra). DNA molecules extend in the nanochannel to 60–90% of their contour length, depending on solution conditions and the size of the nano-fabricated features. Sub-100 nm confinement yields up to 90% polymer extension, corresponding to the Odijk regime of confinement defined by deflection of the polymer off the nanochannel walls.

Excess solution is removed from the chuck inlet chamber before pipetting in subsequent reagents. The reagent is generally diluted in 0.5x TBE with the appropriate antioxidation reagents (BME or PCA/PCD). After inserting reagents in the chuck chamber, negative pressure is applied to the chamber via the outlet to load reagent into the microchannels.

3 Results and Discussion

3.1 Visualization of DNA extension and brightness change in response to buffer exchange

We visualize the dynamic effect of increasing ionic strength on DNA–YOYO-1 complexes confined within nanogrooves to demonstrate our nanofluidic platform. In the literature, there exist variable reports on the effects that both YOYO-1, ionic strength and type of ion can have on the physical properties of DNA (Ref. 33 and Ref. 12–15 and 18–21 therein).

Here, we increase the ionic strength by introducing buffer with additional sodium chloride, which screens electrostatic interactions between charges (3a,b). We time resolve the effect of modifying the ionic strength of solution upon DNA extension and brightness. DNA are in solution and experience the applied lateral confinement of the nanogroove walls and vertical confinement of the CLiC chamber roof.

Fluorescent images are recorded during buffer exchange and later fitted to determine extension L and integrated intensity I as a function of time, using prior analysis methods in Ref. 34 (3c). We observe DNA length to decrease when a higher–ionic-strength buffer is introduced and to stabilize to a new value (3d). On a comparatively longer timescale, we

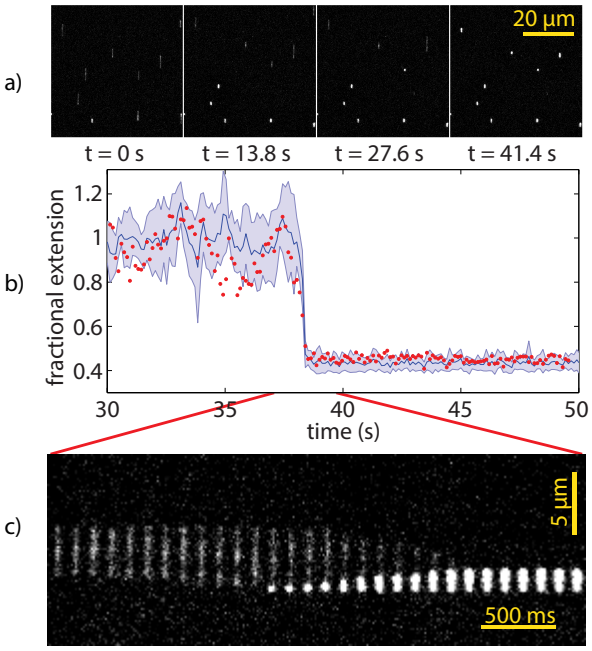

Fig. 4 DNA extension and condensation in response to cetyl trimethylammonium chloride (CTMA). **a)** Images of confined Cy3-labeled DNA in nanochannels whose surfaces have been pre-treated with hydrophobic silane (FOCS) and PVP; images are acquired after introduction of CTMA. Condensation of DNA proceeds with the diffusion front of CTMA. **b)** Mean fractional extension of 7 DNA molecules undergoing compaction. Trajectories have been aligned to maximize correlation of the signals. Dramatic decrease in extension is accompanied by a decrease in fluctuation of lengths, as indicated by the shaded region representing the standard deviation of lengths. Red dots indicate the trajectory of a single representative molecule. **c)** Kymograph montage of a representative DNA molecule (which corresponds to the red dots) through the compaction transition, demonstrating temporal and spatial resolution of compaction dynamics.

observe the DNA intensity to also decrease and then stabilize. In time-resolving the change in DNA length and brightness simultaneously we observe 1) an immediate decrease in DNA length, which we interpret to be primarily due to introducing ions which serve to partially screen the self-repulsive polymer from itself and 2) a subsequent decrease in brightness due to releasing YOYO-1 fluorophores intercalated within the DNA backbone, which also serves to stiffen the polymer.

YOYO-1 dye is electrostatically coupled to the negatively charged backbone, and its bis-intercalating fluorescent ring structures interleave with the π-stacked bases. When it intercalates in this fashion, the fluorescence intensity is increased by over 1000 fold[35,36]. Thus when we screen the electrostatic interactions responsible for the DNA–YOYO-1 binding stability, it is expected that we see a corresponding decrease in fluorescence intensity.

The decrease in DNA extension caused by increasing the concentration of cations results from "screening" the repulsion force experienced by the negative charges along the length of the DNA. This lowered repulsion decreases the DNA stiffness, and in turn decreases the persistence length and the extension. However, it is known that intercalation of YOYO-1 dye also has an effect on DNA contour length (and therefore extension). The literature is divided on its effect on persistence length, whether it is constant or decreases with YOYO-1 intercalation[33]. Discrepencies in findings arise from the difficulty of performing measurements in an equilibrium state, and a failure to control for this equilibration process. Nontheless, where a decrease is measured, it is suggested that YOYO-1 decreases persistence length by introducing local kinks along the DNA chain[37].

Our experiment suggests a new way to separate simultaneous effects on DNA extension in a temporally resolved measurement of DNA conformational dynamics. We propose that the YOYO-molecule takes longer to dissociate from the DNA basepairs due to pi-stacking of the ring structures on its bis-intercalating ends with the bases[30,31] . We see no evidence that persistence lengths increases with decreasing YOYO-1 bound, as the length plateaus before the YOYO-1 intercalation equilibrates.

3.2 Visualization of DNA condensation in response to introduction of a cationic surfactant

To effect the compaction of DNA, we used the surfactant cetyl trimethyl ammonium chloride (CTMA), which has a positive head group and a long hydrophobic tail. The positive charges bind along the length of the DNA and cause the DNA to condense and eventually precipitate[38]. We explore the dynamics of this condensation transition with single-molecule resolution. To suppress interactions with the walls of the nanochannel, we treat the glass with the fluorinated silane FOCS, which makes a hydrophobic, inert layer, and to avoid the effects of CTMA on YOYO-1 intercalation and thus the intensity and extension of the DNA, we labeled the λ-phage DNA covalently with Cy3 moieties.

After introduction of the CTMA buffer, we see a striking compaction transition occur, progressing towards the center of the chamber from the microchannels, representing the diffusing front of the CTMA region (Figure 4). As the CTMA buffer approaches the DNA, the DNA is pulled towards the interface of the buffers, and compaction proceeds along the length of the DNA within one second of initial nucleation. The compacted state is characterized as a 2.5-fold increase in local intensity as well as decrease in polymer length to 40% of its initial value. Eventually the compacted molecules adsorb onto the surface and do not exhibit resolvable fluctuations in intensity

or length (Fig. 4b,c). In the compacted state, the DNA is still confined by the nanogroove and top surfaces: rather than compacting into a spherical globule, as seen in other experiments, we see what looks suggestively to be a chain of smaller globules aligned with the nanochannel, corresponding with the the de Gennes 'blob' model for polymers at confinement $\gg$ their persistence length, L_p.

In the de Gennes regime of confinement, the mean extension $< R_z >$ of a polymer is given by [39]

$$< R_z > \simeq L_c \left(\frac{w L_p}{h^2} \right)^{1/3} \quad (1)$$

where L_c is the polymer's contour length, w is its width, and h is the confinement dimension. When a channel is rectangular, h is taken to be the geometric mean of the width and height [40]. We estimate our channels in the experiment with CTMA to be 50nm by 70nm (50nm for the channel plus 20nm-tall posts), yielding $h = 59$nm. The contour length of λ DNA is 16.49 μm. The width is typically estimated at 5 nm, but CTMA is likely to reduce this by shielding negative charges and distrupting the hydration shell around DNA, and so we very roughly estimate the effective width in the presence of CTMA as 3 nm.. Inserting these values into Equation 1 yields a mean L_p of 2.4 nm with a standard error of 0.4 nm. This result amounts to a $\sim$20-fold reduction in L_p from its usual value of 50 nm, in surfactant-free aqueous solutions of ionic strengths typical in biophysical experiments. In our experiment, the de Gennes model is not entirely appropriate, however, as the true conformation of the polymer is likely more complex, as it is able to spill out at the top of the nanochannel and additionally adsorb to the surface, and the FOCS and PVP treatment may affect the effective confinement dimensions, so our reported L_p should be considered a very approximate estimate.

3.3 Conclusions

This work demonstrates a new, glass-based nanofluidic platform to control and visualize reactions in small spaces. It advances the CLiC approach to gently confining and extending biopolymers and biomolecules within nanoscale environments by enabling the capability to temporally control reagent insertion within the CLiC nanoslit. Further, it enables real-time visualization of subsequent dynamics and reactions with single-fluorophore sensitivity because embedded nanotopographies are fabricated on thin coverslips compatible with high-NA oil-immersion objectives as opposed to thicker slides that require lower-NA water-immersion objectives [34]. CLiC confinement allows custom control over confined polymer shape on the nanoscale, allowing us to template DNA before reacting it, which is useful for conformation-dependent processes such as ligation. High resolution allows us to track the individual trajectories of each and every molecule's interactions. High-throughput device affords statistics limited only by the resolution and field-of-view of the detection system, labels, and camera.

Furthermore, with the nano confinement environment formed by simple coverslip deformation, templated and chemically treated DNA could be recovered from the experiment for further analysis in higher-resolution imaging systems, such as SEM or AFM. For instance, deposition of molecular complexes onto surfaces could be performed after dynamics of molecules are observed in solution. Large numbers of deposited complexes, with potentially controlled orientations, could be analyzed using e.g. SEM or AFM systems following device-disassembly. Further, of great interest to the biotechnology sector, this platform could be applied to visualize, diagnose and optize important enzymatic reactions in real time, such as ligation and labeling reaction steps which often represent low-yield steps in sample-preparation tools for sequencing platforms. Overall, this nanofluidic platform can be used to explore a wide range of fascinating chemical interactions of interest to biological, biotechnological, biophysical, chemical, and materials science research communities.

Acknowledgements

The authors thank the National Science and Engineering Research Council of Canada as well as ZSGenetics and McGill University for financial support for this research. DB GH and FS thank the McGill Nanotools Facility, INRS Fabrication Facility, and Center for Physics of Materials group for equipment and tool usage and technician support. Further, we thank Stephen Michnick and Vincent Tabard-Cossa for critical readings of this manuscript.

References

1 A. A. Deniz, S. Mukhopadhyay and E. A. Lemke, *Journal of The Royal Society Interface*, 2008, **5**, 15–45.
2 S. L. Levy and H. G. Craighead, *Chem. Soc. Rev.*, 2010, **39**, 1133–1152.
3 S. ichi Nakano, D. Miyoshi and N. Sugimoto, *Chemical Reviews*, 2014, **114**, 2733–2758.
4 W. Reisner, J. N. Pedersen and R. H. Austin, *Reports on Progress in Physics*, 2012, **75**, 106601.
5 J. F. Thompson and P. M. Milos, *Genome Biology*, 2011, **12**, 1–10.
6 M. L. Metzker, *Nat Rev Genet*, 2009, **11**, 31–46.
7 F. Persson and J. O. Tegenfeldt, *Chem. Soc. Rev.*, 2010, **39**, 985–999.
8 D. Dulin, J. Lipfert, M. C. Moolman and N. H. Dekker, *Nat. Rev. Genet.*, 2013, **14**, 9–22.

9 P. V. Cornish and T. Ha, *ACS Chemical Biology*, 2007, **2**, 53–61.

10 C. Joo, H. Balci, Y. Ishitsuka, C. Buranachai and T. Ha, *Annu. Rev. Biochem.*, 2008, **77**, 51–76.

11 M. Capitanio and F. S. Pavone, *Biophysical journal*, 2013, **105**, 1293–1303.

12 K. C. Neuman and A. Nagy, *Nature methods*, 2008, **5**, 491.

13 I. De Vlaminck and C. Dekker, *Annual review of biophysics*, 2012, **41**, 453–472.

14 S. Kasas, G. Longo and G. Dietler, *Journal of Physics D: Applied Physics*, 2013, **46**, 133001.

15 R. K. Neely, J. Deen and J. Hofkens, *Biopolymers*, 2011, **95**, 298–311.

16 M. Xiao, A. Phong, C. Ha, T.-F. Chan, D. Cai, L. Leung, E. Wan, A. L. Kistler, J. L. DeRisi, P. R. Selvin and P.-Y. Kwok, *Nucleic Acids Research*, 2007, **35**, e16.

17 E. Y. Chan, N. M. Goncalves, R. A. Haeusler, A. J. Hatch, J. W. Larson, A. M. Maletta, G. R. Yantz, E. D. Carstea, M. Fuchs, G. G. Wong, S. R. Gullans and R. Gilmanshin, *Genome Research*, 2004, **14**, 1137–1146.

18 H. Zohar and S. J. Muller, *Nanoscale*, 2011, **3**, 30273039.

19 W. Cai, H. Aburatani, V. P. Stanton, D. E. Housman, Y. K. Wang and D. C. Schwartz, *Proceedings of the National Academy of Sciences*, 1995, **92**, 5164–5168.

20 K. D. Dorfman, S. B. King, D. W. Olson, J. D. P. Thomas and D. R. Tree, *Chemical Reviews*, 2013, **113**, 2584–2667.

21 F. Baldessari and J. G. Santiago, *Journal of Nanobiotechnology*, 2006, **4**, 1–6.

22 O. B. Bakajin, T. A. J. Duke, C. F. Chou, S. S. Chan, R. H. Austin and E. C. Cox, *Phys. Rev. Lett.*, 1998, **80**, 2737–2740.

23 A. Alrifaiy, O. A. Lindahl and K. Ramser, *Polymers*, 2012, **4**, 1349.

24 S. R. Leslie, A. P. Fields and A. E. Cohen, *Analytical Chemistry*, 2010, **82**, 6224–6229.

25 D. Berard, C. M. J. McFaul, J. S. Leith, A. K. J. Arsenault, F. Michaud and S. R. Leslie, *Rev. Sci. Instrum.*, 2013, **84**, 103704.

26 D. R. Tree, Y. Wang and K. D. Dorfman, *Phys. Rev. Lett.*, 2013, **110**, 208103.

27 H. Lee, D. Ham and R. Westervelt, *CMOS Biotechnology*, Springer, 2007.

28 B. Alberts, A. Johnson, J. Lewis, M. Raff, K. Roberts and P. Walter, *Molecular Biology of the Cell (3rd ed.)*, Garland Science: New York, NY, 2002.

29 N. V. Hud and I. D. Vilfan, *Annual Review of Biophysics and Biomolecular Structure*, 2005, **34**, 295–318.

30 A. Sischka, K. Toensing, R. Eckel, S. D. Wilking, N. Sewald, R. Ros and D. Anselmetti, *Biophysical journal*, 2005, **88**, 404–411.

31 M. Reuter and D. T. Dryden, *Biochemical and biophysical research communications*, 2010, **403**, 225–229.

32 T. Odijk, *Macromolecules*, 1986, **19**, 2313.

33 B. Kundukad, J. Yan and P. S. Doyle, *Soft matter*, 2014, **10**, 9721–9728.

34 D. J. Berard, F. Michaud, S. Mahshid, M. J. Ahamed, C. M. J. McFaul, J. S. Leith, P. Bérubé, R. Sladek, W. Reisner and S. R. Leslie, *Proc Natl Acad Sci U S A*, 2014, **111**, 13295–300.

35 H. S. Rye, S. Yue, D. E. Wemmer, M. A. Quesada, R. P. Haugland, R. A. Mathies and A. N. Glazer, *Nucleic Acids Research*, 1992, **20**, 2803–2812.

36 H. Rye, J. Dabora, M. Quesada, R. Mathies and A. Glazer, *Analytical Biochemistry*, 1993, **208**, 144–150.

37 M. Maaloum, P. Muller and S. Harlepp, *Soft Matter*, 2013, **9**, 11233–11240.

38 S. M. Mel'nikov, V. G. Sergeyev and K. Yoshikawa, *Journal of the American Chemical Society*, 1995, **117**, 2401–2408.

39 J. O. Tegenfeldt, C. Prinz, H. Cao, S. Chou, W. W. Reisner, R. Riehn, Y. M. Wang, E. C. Cox, J. C. Sturm, P. Silberzan and R. H. Austin, *Proceedings of the National Academy of Sciences of the United States of America*, 2004, **101**, 10979–10983.

40 Y. Wang, D. R. Tree and K. D. Dorfman, *Macromolecules*, 2011, **44**, 6594–6604.